Geomorphic Constraints on Fault Geometry and Seismic Slip Deficit in the Himalaya

1 Introduction

Many Himalayan rivers contain zones of anomalously high gradient that cannot be explained by variations in rock strength [10]. The persistent spatial correlation between these steepened reaches and mapped faults strongly suggests that the gradients reflect differential tectonic uplift of the High Himalayas rather than lithologic contrasts [10].

River profiles encode this uplift spatially. Under the stream power incision model, channel slope integrates the rock uplift rate over distance [1]. Therefore, spatial variations in uplift produce diagnostic signatures in channel morphology. Meade [7] showed that channel convexity in the Himalayas may record earthquake-cycle imbalance—permanent retention of interseismic strain that is not fully recovered coseismically.

Quantifying these geomorphic markers matters for two reasons. First, they constrain long-term seismic deficits. Bilham and Ambraseys [3], Bilham et al. [4] estimated that coseismic moment release has lagged behind accumulation by ~75% over the past 500 years. Second, they offer an alternative method for mapping subsurface fault geometry using freely available satellite topography, which is particularly valuable in the Himalayas where direct fault imaging is hindered by rugged terrain and limited access.

However, modeling crustal deformation from fault slip to surface signatures has historically been divided between two frameworks. Structural geology uses geometric kinematic models (rigid blocks separated by faults and folds), while seismology and geodesy use continuum mechanics models (elastic dislocations in a half-space). Avouac [2] noted qualitatively that the long-term average of transient earthquake cycles should recover the structural deformation field, and other studies [5, 12] have explored connections between the two. Yet a formal equivalence has not been established. Structural models cannot account for transient elastic strains within the earthquake cycle, and standard elastic dislocation models cannot directly produce finite, long-term mountain building. Demonstrating their equivalence is therefore essential: it enables modeling long-term orogenesis while incorporating the potentially unbalanced kinematics of individual earthquake cycles.

2 Methods

2.1 Elastic dislocation model

We model fault slip and fold growth using Volterra dislocations in a semi-infinite elastic medium [6, 13]. A Volterra dislocation prescribes a uniform displacement discontinuity $\mathbf{b}$ (the Burgers vector) across an internal surface Σ. The discontinuity generates stress singularities only along the dislocation line σ bounding Σ; stresses remain continuous everywhere else [6, eq. 1.6]. In the two-dimensional plane-strain case, the dislocation line extends to infinity along strike, reducing the problem to that of an edge dislocation whose Burgers vector lies in the cross-sectional plane [6, Section 1-2]. The surface displacement from a finite fault segment is obtained by superposing two edge dislocations of opposite sign at the segment endpoints [8, 12].

We prove that the structural (kinematic) velocity field is the unique solution of the elastic boundary-value problem (BVP), first for a single planar fault and then for a general fault-bend fold.

2.2 Infinite planar fault

Consider a planar fault Σ dipping at angle δ and extending from the free surface to infinite depth in a homogeneous, isotropic, semi-infinite elastic medium. Prescribe a Volterra dislocation with Burgers vector $\mathbf{b} = s(\cos\delta,\, \sin\delta)^T$. The structural model assigns a rigid translation $\mathbf{b}$ to the hanging wall and zero displacement to the footwall:

$$\mathbf{u}(\mathbf{x}) = \mathbf{b}\, H(\boldsymbol{\nu}\cdot\mathbf{x}), \tag{1}$$

where H is the Heaviside function and $\boldsymbol{\nu}$ is the outward normal to Σ. This field is piecewise constant, so the strain ε_{ij} and stress τ_{ij} vanish identically on each side of Σ. Equilibrium, the free-surface condition $\tau_{2j} = 0$ at $x_2 = 0$, stress continuity $\tau^+_{kl}\nu_l = \tau^-_{kl}\nu_l = 0$ across Σ, and the prescribed displacement discontinuity $\Delta\mathbf{u} = \mathbf{b}$ are therefore all satisfied. By uniqueness of the Volterra BVP [6, 13], the structural field *is* the elastic solution.

For faults of finite depth D, the equivalence holds approximately. The elastic surface displacement from a single edge dislocation at depth d, with the dislocation line at horizontal position ξ_1 and the fault dipping at angle δ, is [11, eq. 3.70]

$$u_2(x_1,\, x_2 = 0) = -\frac{s}{\pi}\left[\sin\delta\, \tan^{-1}(\zeta) + \frac{\cos\delta + \zeta\sin\delta}{1+\zeta^2}\right], \qquad \zeta \equiv \frac{x_1 - \xi_1}{d}. \tag{2}$$

A finite fault segment from the surface to depth D is modeled by superposing two such dislocations of opposite sign at the segment endpoints [11, Section 3.3.1], a surface-breaking dislocation at $(\xi_1,\, d) = (0,\, 0)$ and a compensating dislocation at $(D\cot\delta,\, D)$. As $d \to 0$, the surface dislocation reduces to a step function $u_2^{(0)} = (s\sin\delta/2)\ \mathrm{sgn}(x_1)$, while the deep dislocation produces a smooth field parametrized by $\zeta_D = (x_1 - D\cot\delta)/D$. For any fixed observation point x_1, as $D \to \infty$,

$$\zeta_D = \frac{x_1}{D} - \cot\delta \;\longrightarrow\; -\cot\delta, \tag{3}$$

so the deep dislocation's contribution approaches a spatially uniform constant $C(\delta)$, with corrections of order $O(x_1/D)$. Because the deep endpoint recedes to infinite distance, all surface points view it from the same angle $\zeta \to -\cot\delta$, and the deep dislocation degenerates into a rigid-body translation. Pinning the displacement to a nearby footwall reference $x_{\mathrm{fw}} < 0$ with $|x_{\mathrm{fw}}| \ll D$ removes this common-mode constant,

$$\begin{aligned} u_2(x_1) - u_2(x_{\mathrm{fw}}) &= \left[\frac{s\sin\delta}{2} + C + O\!\left(\frac{x_1}{D}\right)\right] - \left[-\frac{s\sin\delta}{2} + C + O\!\left(\frac{x_{\mathrm{fw}}}{D}\right)\right] \\ &= s\sin\delta + O\!\left(\frac{L}{D}\right), \end{aligned} \tag{4}$$

where $L = \max(|x_1|,\, |x_{\mathrm{fw}}|)$ is the extent of the observation window. The constant $C(\delta)$ cancels identically, and the residual is set by the ratio of the observation scale to the fault depth. The cancellation requires both the observation and reference points to lie in the same angular sector relative to the deep endpoint, i.e., $|x_{\mathrm{fw}}|/D \to 0$; if $|x_{\mathrm{fw}}| \sim D$, the deep dislocation evaluates to different constants at the two locations, and the residual saturates rather than decaying. Figure 1 verifies this $O(1/D)$ convergence numerically for a 30° planar thrust.

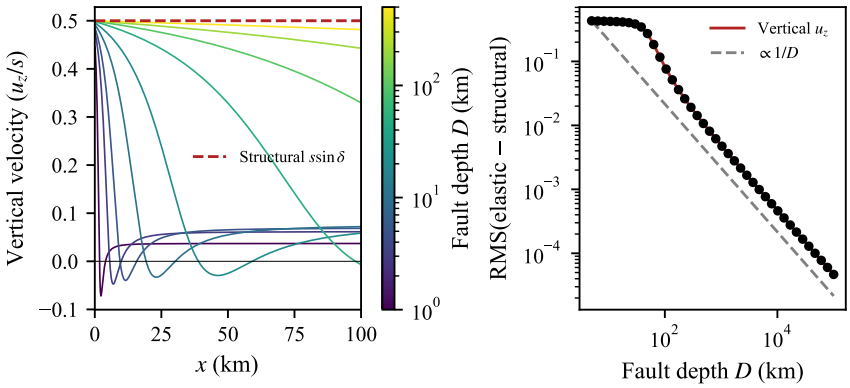

Figure 1: Convergence of the elastic vertical displacement to the structural prediction for a 30° planar thrust with unit slip. *Left:* Elastic vertical velocity profiles for fault depths from 1 to 10^5 km (viridis colormap), converging to $s \sin 30° = 0.5$ (dotted line). *Right:* RMS misfit between elastic and structural vertical fields as a function of fault depth D, evaluated over $x \in [0, 100]$ km, following the $O(1/D)$ reference slope.

2.3 Non-planar fault geometry (fault-bend fold)

Natural faults are rarely planar. Where a fault changes dip, the hanging wall must deform to accommodate the change in slip direction. In structural geology, a fault composed of N planar segments meeting at $N-1$ kink points is known as a fault-bend fold. The hanging wall is partitioned into rigid domains separated by axial surfaces. Block i overlies segment i with dip θ_i. Assuming a uniform slip rate s parallel to each segment, block i moves at velocity

$$\mathbf{v}_i = s \begin{pmatrix} \cos\theta_i \\ \sin\theta_i \end{pmatrix}. \tag{5}$$

The velocity jump across the axial surface separating blocks $i-1$ and i is

$$\Delta\mathbf{v}_i = \mathbf{v}_i - \mathbf{v}_{i-1} = s \begin{pmatrix} \cos\theta_i - \cos\theta_{i-1} \\ \sin\theta_i - \sin\theta_{i-1} \end{pmatrix}. \tag{6}$$

Applying sum-to-product identities with $\Delta\theta = \theta_i - \theta_{i-1}$ and $\bar{\theta} = (\theta_i + \theta_{i-1})/2$ gives

$$\Delta\mathbf{v}_i = 2s \sin\left(\frac{\Delta\theta}{2}\right) \begin{pmatrix} -\sin\bar{\theta} \\ \cos\bar{\theta} \end{pmatrix} = 2s \sin\left(\frac{\Delta\theta}{2}\right) \hat{\mathbf{a}}, \tag{7}$$

where $\hat{\mathbf{a}} = (-\sin\bar{\theta}, \cos\bar{\theta})$ is the unit tangent to the axial surface. This result has a simple geometric interpretation: the unit tangent vectors $\hat{\mathbf{t}}_1$ and $\hat{\mathbf{t}}_2$ of the two segments have equal magnitude, so they form a rhombus with the origin. The diagonals of a rhombus are perpendicular, so $\hat{\mathbf{t}}_2 - \hat{\mathbf{t}}_1$ is perpendicular to the bisector $\hat{\mathbf{t}}_1 + \hat{\mathbf{t}}_2$ and therefore parallel to the axial surface $\hat{\mathbf{a}}$.

Equation (7) shows that the velocity jump is *purely tangential* to the axial surface—there is no tensile (opening) component. More generally, if adjacent segments carry different slip rates $s_{i-1} \neq s_i$, the velocity jump decomposes as

$$\text{shear:} \quad \Delta\mathbf{v}_i \cdot \hat{\mathbf{a}} = (s_{i-1} + s_i) \sin\left(\frac{\Delta\theta}{2}\right), \tag{8}$$

$$\text{tensile:} \quad \Delta\mathbf{v}_i \cdot \hat{\mathbf{n}} = (s_i - s_{i-1}) \cos\left(\frac{\Delta\theta}{2}\right), \tag{9}$$

where $\hat{\mathbf{n}} = (\cos\bar{\theta}, \sin\bar{\theta})$ is the unit normal to the axial surface. In general, both components are nonzero, and earlier implementations accordingly include both dip-slip and tensile dislocations on the axial surface [8, 12]. However, mass conservation in a balanced kink-band fold requires every segment to carry the same slip rate ($s_{i-1} = s_i = s$), which causes the tensile component (9) to vanish identically.

2.4 Burgers vector closure and completion of the proof

At a fault bend, three dislocation surfaces meet with Burgers vectors $\mathbf{b}_{\text{in}} = \mathbf{v}_{i-1}$ (incoming fault), $\mathbf{b}_{\text{out}} = \mathbf{v}_i$ (outgoing fault), and $\mathbf{b}_{\text{axial}} = \Delta\mathbf{v}_i$ (axial surface). These satisfy

$$\mathbf{b}_{\text{in}} + \mathbf{b}_{\text{axial}} - \mathbf{b}_{\text{out}} = \mathbf{v}_{i-1} + (\mathbf{v}_i - \mathbf{v}_{i-1}) - \mathbf{v}_i = \mathbf{0}. \tag{10}$$

This closure condition $\sum \mathbf{b} = \mathbf{0}$ ensures that no uncompensated singularity exists at the junction.

The structural velocity field partitions the half-space into $N + 1$ rigid domains (the stationary footwall and N hanging-wall blocks):

$$\mathbf{u}(\mathbf{x}) = \begin{cases} \mathbf{v}_i & \text{if } \mathbf{x} \text{ lies in block } i, \\ \mathbf{0} & \text{if } \mathbf{x} \text{ lies in the footwall.} \end{cases} \tag{11}$$

As for the single planar fault, this field is piecewise constant, so $\varepsilon_{ij} = 0$ and $\tau_{ij} = 0$ in every block. Equilibrium, free-surface, and stress-continuity conditions are all satisfied. The displacement discontinuities match the prescribed Burgers vectors of the fault segments and axial surfaces, and the closure condition $\sum \mathbf{b} = \mathbf{0}$ holds at every junction. By uniqueness, the structural field is the elastic solution.

2.5 Partitioning the earthquake cycle

The equivalence theorem lets us partition the earthquake cycle for a fault-bend fold using linear superposition. The dislocation network Σ_{total} comprises two categories of surfaces, fault segments and axial planes. By the equivalence theorem, the long-term velocity field equals the structural velocity

$$\mathbf{v}_{\text{long-term}} \equiv \mathbf{v}_{\text{struct}} = \mathbf{v}(\Sigma_{\text{fault}}) + \mathbf{v}(\Sigma_{\text{axial}}), \tag{12}$$

where $\mathbf{v}(\Sigma)$ denotes the elastic surface velocity produced by slip rate s on the surface set Σ. In the slip-deficit framework [9], each surface is either locked or creeping, giving $\Sigma_{\text{total}} = \Sigma_{\text{locked}} \cup \Sigma_{\text{creep}}$. The cycle-averaged kinematic budget is

$$\mathbf{v}_{\text{long-term}} = \mathbf{v}(\Sigma_{\text{locked}}) + \mathbf{v}(\Sigma_{\text{creep}}), \tag{13}$$

where the first term is the cycle-averaged coseismic contribution and the second is the interseismic velocity.

Fault-bend fold models represent the fault as a finite number of planar segments joined at discrete, sharp bends. Each kink concentrates all folding deformation onto a single axial surface, whose dislocation produces a step-function discontinuity in $\mathbf{v}_{\text{struct}}$. Consider a fault with N segments where the first k are locked. Let $\Sigma^{(\text{co})}_{\text{axial}} \subseteq \Sigma_{\text{axial}}$ denote the axial surfaces assigned to the coseismic term and $\Sigma^{(\text{in})}_{\text{axial}} = \Sigma_{\text{axial}} \setminus \Sigma^{(\text{co})}_{\text{axial}}$ those assigned to the interseismic term, so that

$$\mathbf{v}_{\text{coseismic}} = \mathbf{v}(\Sigma^{(\text{locked})}_{\text{fault}}) + \mathbf{v}(\Sigma^{(\text{co})}_{\text{axial}}), \tag{14}$$

$$\mathbf{v}_{\text{interseismic}} = \mathbf{v}(\Sigma^{(\text{creep})}_{\text{fault}}) + \mathbf{v}(\Sigma^{(\text{in})}_{\text{axial}}). \tag{15}$$

The fault-segment contributions are spatially smooth, but each axial dislocation produces a step-function velocity jump at the surface. Because $\Sigma^{(\text{co})}_{\text{axial}} \cup \Sigma^{(\text{in})}_{\text{axial}} = \Sigma_{\text{axial}}$ is fixed, transferring an axial surface from one group to the other moves the discontinuity but cannot eliminate it. No partition of Σ_{axial} yields smooth fields for both the coseismic and interseismic components simultaneously. This trade-off is an artifact of

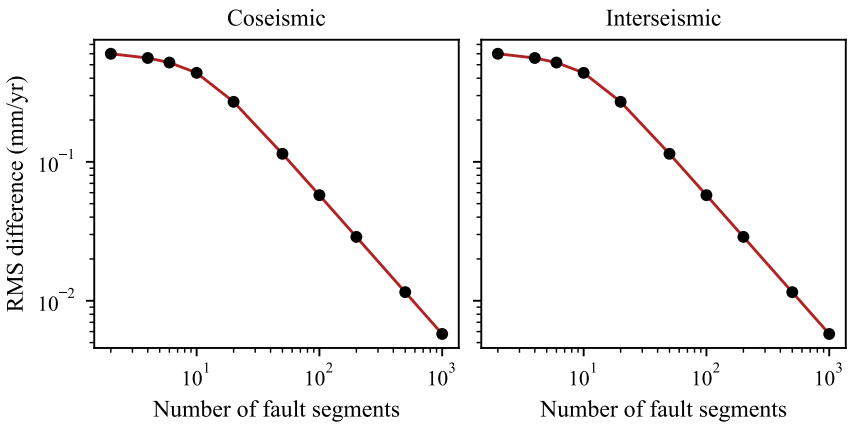

Figure 2: RMS difference between two end-member axial surface partitioning strategies as a function of fault discretisation. A two-segment fault with a single kink is progressively refined using C^2 quintic smoothing and equal arc-length resampling, with the lock/creep transition held near $x \approx 50$ km. Both coseismic and interseismic differences decrease identically, confirming that the partitioning choice is a discretisation artifact that vanishes for smooth fault geometries.

discretisation: for a fault with smooth, continuously varying curvature, the folding is distributed rather than concentrated at discrete kinks, and no discrete axial surfaces arise. As the number of fault segments increases the individual fold contributions become negligible and the two end-member assignments—$\Sigma_{\text{axial}}^{(\text{co})} = \Sigma_{\text{axial}}$ versus $\Sigma_{\text{axial}}^{(\text{co})} = \varnothing$—converge (Figure 2), with the RMS difference decreasing monotonically. In the smooth-fault limit the decomposition depends only on which fault segments are locked.

2.6 Geomorphic forcing from the earthquake cycle

In bedrock incision models such as the stream power equation [1, 15],

$$\frac{\partial z}{\partial t} = U(x) - KA^m S^n, \tag{16}$$

topography evolves in response to a rock uplift rate $U(x)$. Rivers integrate the time-averaged permanent vertical motion over many seismic cycles [14]. Let s_c denote the average coseismic slip rate on the locked zone. The cycle-averaged tectonic velocity is

$$\mathbf{v}_{\text{cycle}} = \mathbf{v}(\Sigma_{\text{creep}};\, s) + \mathbf{v}(\Sigma_{\text{locked}};\, s_c). \tag{17}$$

Balanced cycle ($s_c = s$). If the seismic cycle is perfectly balanced, the average coseismic slip rate equals the tectonic loading rate:

$$\mathbf{v}_{\text{cycle}} = \mathbf{v}(\Sigma_{\text{creep}};\, s) + \mathbf{v}(\Sigma_{\text{locked}};\, s) = \mathbf{v}(\Sigma_{\text{total}};\, s) \equiv \mathbf{v}_{\text{struct}}. \tag{18}$$

The uplift field is identical to the structural model. Topography reflects pure fault-bend folding.

Unbalanced cycle ($s_c < s$). If the locked zone releases less slip than it accumulates, a permanent slip deficit $s_{\text{def}} = s - s_c$ remains:

$$\begin{aligned} \mathbf{v}_{\text{cycle}} &= \mathbf{v}(\Sigma_{\text{creep}};\, s) + \mathbf{v}(\Sigma_{\text{locked}};\, s - s_{\text{def}}) \\ &= \mathbf{v}_{\text{struct}} - \mathbf{v}(\Sigma_{\text{locked}};\, s_{\text{def}}). \end{aligned} \tag{19}$$

The uplift field is no longer purely structural but is modified by an elastic residual from unreleased slip. Because $\mathbf{v}(\Sigma_{\text{locked}};\, s_{\text{def}})$ is spatially localized, this produces differential uplift—exactly the signal recorded by Himalayan river profiles.

References

[1] R. S. Anderson and S. P. Anderson. *Geomorphology: the mechanics and chemistry of landscapes*. Cambridge University Press, 2010.

[2] J.-P. Avouac. Mountain building, erosion, and the seismic cycle in the nepal himalaya. *Advances in geophysics*, 46:1–80, 2003.

[3] R. Bilham and N. Ambraseys. Apparent himalayan slip deficit from the summation of seismic moments for himalayan earthquakes, 1500–2000. *Current science*, pages 1658–1663, 2005.

[4] R. Bilham, V. K. Gaur, and P. Molnar. Himalayan seismic hazard. *Science*, 293(5534):1442–1444, 2001.

[5] L. Dal Zilio, G. Hetényi, J. Hubbard, and L. Bollinger. Building the himalaya from tectonic to earthquake scales. *Nature Reviews Earth & Environment*, 2(4):251–268, 2021.

[6] T. Maruyama. 16. statical elastic dislocations in an infinite and semi-infinite medium. *Bull. Earthq. Res. Inst*, 42:289–368, 1964.

[7] B. J. Meade. The signature of an unbalanced earthquake cycle in himalayan topography? *Geology*, 38 (11):987–990, 2010.

[8] B. J. Meade. CoInterFaultFold2D: Coseismic, interseismic, and long-term deformation associated with fault-bend folds. `https://github.com/brendanjmeade/CoInterFaultFold2D`, 2024. Software.

[9] J. C. Savage. A dislocation model of strain accumulation and release at a subduction zone. *Journal of Geophysical Research: Solid Earth*, 88(B6):4984–4996, 1983.

[10] L. Seeber and V. Gornitz. River profiles along the himalayan arc as indicators of active tectonics. *Tectonophysics*, 92(4):335–367, 1983.

[11] P. Segall. *Earthquake and Volcano Deformation*. Princeton University Press, 2010.

[12] B. Souter and B. Hager. Fault propagation fold growth during the 1994 northridge, california, earthquake? *Journal of Geophysical Research: Solid Earth*, 102(B6):11931–11942, 1997.

[13] J. Steketee. On volterra's dislocations in a semi-infinite elastic medium. *Canadian Journal of Physics*, 36(2):192–205, 1958.

[14] K. X. Whipple and B. J. Meade. Orogen response to changes in climatic and tectonic forcing. *Earth and Planetary Science Letters*, 243(1-2):218–228, 2006.

[15] K. X. Whipple and G. E. Tucker. Dynamics of the stream-power river incision model: Implications for height limits of mountain ranges, landscape response timescales, and research needs. *Journal of Geophysical Research: Solid Earth*, 104(B8):17661–17674, 1999.